ELSEVIER

Nuclear Instruments and Methods in Physics Research A 415 (1998) 218–228

NUCLEAR INSTRUMENTS & METHODS IN PHYSICS RESEARCH Section A

Induction accelerator architectures for heavy-ion fusion[1]

J.J. Barnard[a,*], R.O. Bangerter[b], A. Faltens[b], T.J. Fessenden[b], A. Friedman[a], E.P. Lee[b], B.G. Logan[a], S.M. Lund[a], W. Meier[a], W.M. Sharp[a], S.S. Yu[b]

[a] *Lawrence Livermore National Laboratory, Livermore, CA 94550, USA*
[b] *Lawrence Berkeley National Laboratory, Berkeley, CA 94720, USA*

Abstract

The approach to heavy-ion-driven inertial fusion studied most extensively in the US uses induction modulators and cores to accelerate and confine the beam longitudinally. The intrinsic peak-current capabilities of induction machines, together with their flexible pulse formats, provide a suitable match to the high peak-power requirement of a heavy-ion fusion target. However, as in the RF case, where combinations of linacs, synchrotrons, and storage rings offer a number of choices to be examined in designing an optimal system, the induction approach also allows a number of architectures, from which choices must be made.

We review the main classes of architecture for induction drivers that have been studied to date. The main choice of accelerator structure is that between the linac and the recirculator, the latter being composed of several rings. Hybrid designs are also possible. Other design questions include which focusing system (electric quadrupole, magnetic quadrupole, or solenoid) to use, whether or not to merge beams, and what number of beams to use – all of which must be answered as a function of ion energy throughout the machine. Also, the optimal charge state and mass must be chosen. These different architectures and beam parameters lead to different emittances and imply different constraints on the final focus. The advantages and uncertainties of these various architectures will be discussed.

Keywords: Heavy-ion fusion; Induction linacs; Inertial fusion; Recirculators

1. Introduction

A number of options using the induction acceleration approach for a heavy-ion driver have been studied and/or reexamined by researchers at the Lawrence Livermore and Lawrence Berkeley National Laboratories (e.g. Refs. [1–4]). The purpose of this paper is to describe four examples of such accelerator concepts that illustrate the variety of approaches being considered, and to give scaling relationships and qualitative reasoning explaining the rationale for the various configurations.

The four example accelerator concepts that will be described are the following: (1) the multiple beamline, single-coreline, quadrupole-focused linac

* Corresponding author.

[1] Work performed under the auspices of the US Department of Energy at LLNL under contract W-7405-ENG-48 and at LBNL by the Director, Office of Energy Research, Advanced Energy Projects Division, US D.O.E. under contract DE-AC03-76SF00098.

0168-9002/98/$19.00
PII: S0168-9002(98)00387-8

(hereafter multi-beam linac); (A coreline is the set of beamlines which thread a common set of induction cores). (2) the recirculator, composed of three rings, and four beamlines throughout; (3) a linac with four beamlines, with low-energy solenoidal focusing, and high energy magnetic quadrupolar focusing (hereafter termed the solenoidal linac); and (4) the multiple coreline, high charge state linac. Fig. 1 schematically illustrates, and Table 1 lists some of the major parameters of, the four architecture concepts.

The multi-beam linac example has 192 beams in a low-energy, electrostatically focused section, followed by a four-to-one merge into a 48-beam magnetically transported section. The main reasons for having large beam numbers are three-fold: First, in the electrostatic section the large beam number maximizes the current transport through a fixed core radius, minimizing the core volume. Second, the large beam number allows a larger ratio of the required final six-dimensional phase-space volume to the initial volume out of the injector. This allows a larger increase in the transverse and parallel normalized emittances, allowing a greater safety factor in permissible emittance dilution. Third, recent LLNL target designs require a large number of beams for symmetry considerations [5].

The recirculator is the only circular accelerator among the four examples. Cost reduction is the main motivation for this approach, achieved through the multiple use of induction cores and quadrupoles during each acceleration sequence using the circular layout. The recirculator is more compact than a multi-beam linac at the same energy. The circumference ~ 2 km is dictated by the radius of curvature of a 10 GeV ion in a ~ 2 T dipole magnetic field (at an average dipole occupancy of 0.33). In the linac approach the maximum accelerating gradient (of 1–2 MV/m) determines the scale of the machine (length ~ 5–10 km at 10 GeV). The size of the induction cores also tends to be reduced in a recirculator, because reuse of the cores allows a smaller accelerating gradient to be used, with an associated reduction in core size.

In the solenoidal linac approach (cf. Ref. [3]), the simplicity of having a small number of beams together with the hope of a lower cost lead to the consideration of solenoids for the low-energy end of the machine [see also Ref. [6]). The different

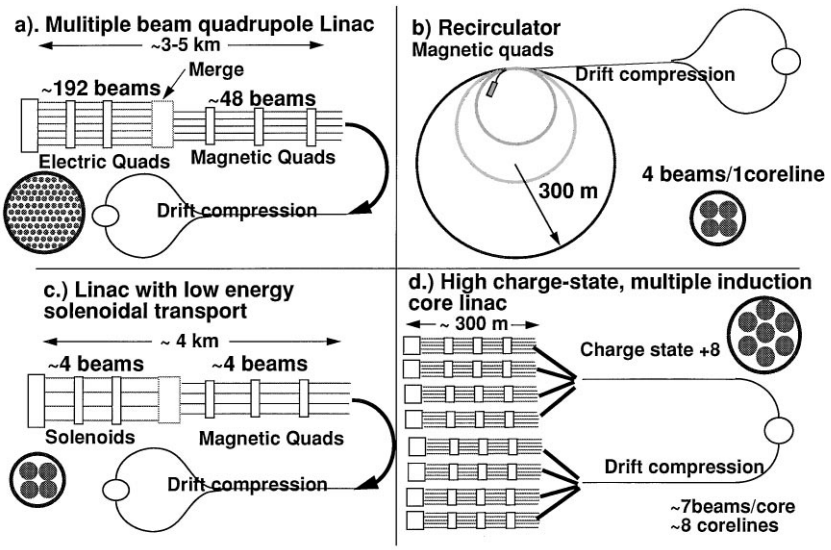

Fig. 1. Four induction accelerator concepts: (a) Multiple-beam quadrupole focused linac; (b) Recirculator, (c) Linac with low-energy solenoidal focusing, and (d) High-charge state multiple coreline linac. Note the cross section of a single coreline is shown with the approximate number of quadrupole focusing channels indicated as dark circles.

Table 1
Summary of parameters of the four accelerator examples

	Multi-beam linac	Recirculator	Solenoidal linac	High-charge-state linac
Reference	[1]	[2]	[3]	[4]
Ion mass	200	200	133	131
Ion charge state	1	1	1	8
Final energy (in all beams)	6.3 MJ	4 MJ	4 MJ	6.5 MJ
Total charge (in all beams)	1.7 mC	0.4 mC	1.0 mC	23.6 mC
Low-energy section[a]				
No. of beamlines	196	4	4	93
No. of corelines	1	1	1	14
Focusing type	Electric quad.	Magnetic quad.	Solenoids	Magnetic quad.
Ion energy	2–100 MeV	3–50 MeV	4–30 MeV	2.65–2200 MeV
Pulse duration	30–4.2 μs	200–30 μs	10–3.7 μs	6.0–0.6 μs
Medium-energy section				
No. of beamlines		4		
No. of corelines		1		
Focusing type		Magnetic quad		
Ion energy		50–1000 MeV		
Pulse duration		30–2.5 ms		
High-energy section				
No. of beamlines	48	4	4	
No. of corelines	1	1	1	
Focusing type	Magnetic quad	Magnetic quad	Magnetic quad	
Ion energy	0.1–4.0 GeV[b]	1.0–10.0 GeV	0.03–4.0 GeV	
Pulse duration	4.2–0.11 μs[b]	2.5–0.25 μs	3.7–0.13 μs	
Bunching/drift compression				
No. of beamlines	48	4	4	93
Pulse duration	110–8 ns[b]	250–10 ns	134–10 ns	600–10 ns

[a]The "low-energy section" of the high-charge-state linac comprises the entire accelerator (i.e. to a total voltage of 275 MV).
[b](In Ref. [1] 32 of the 48 beams form a 4 GeV main pulse, while 16 beams are accelerated to 3 GeV only, forming a prepulse consistent with the target of Ref. [14]. Main pulse parameters are shown.)

scaling of transportable current leads to optimal designs with small numbers of beams.

The fourth example discussed here is that considered in [4], in which there is a reexamination of the use of high-charge-state ions, to drastically reduce the length of the accelerator, but with a proportionate increase in the overall number of beams. By also using multiple corelines, the accelerator could be built in stages, coreline by coreline, with each coreline reaching full energy. This machine is alone among the four examples in terms of its development path. Since each coreline is a prototype of the set of corelines which make up the full accelerator, all accelerator issues could be addressed after completing a single coreline, and at a cost which would be a small fraction of the full machine.

In the remainder of this review, we will describe the major elements of induction accelerators, emphasizing the scaling relationships of the induction cores, focusing elements, and bending elements on the variables which distinguish the four concepts, such as number of beams, pulse duration, accelerating gradient, and charge state. We will also return to the four concepts and explicitly discuss the advantages and key issues associated with each.

2. Induction acceleration and energy loss mechanisms

Acceleration is achieved in all four concepts by the use of a series of induction modules, each module adding an energy increment to the beam. The induction module consists of the induction core, which is an annulus of ferromagnetic material and a modulator, which consists of a set of capacitors or a pulse forming network for energy storage and a switch. The principle is the same as that of a transformer, in which the beam (which threads the core) acts like a "one-turn" secondary of the transformer (see e.g. Ref. [7] for a review). As in the case of a transformer, Faraday's law relates the voltage increment ΔV, and pulse duration Δt to the cross-sectional area of the annulus A and the change in magnetic flux ΔB:

$$\Delta V \Delta t = A \Delta B. \tag{1}$$

Since the total volume of ferromagnetic material (such as Metglas) is a major cost of the accelerator, keeping either the pulse duration short or the voltage increment small is essential to having cores of reasonable areas and volumes. In the linac approaches, a high voltage gradient is desirable to minimize costs. In the recirculator approach, the cores are reused, so the voltage gradient can be reduced and/or pulse durations can be longer. In the recirculator example examined in this paper this flexibility is used to increase the pulse duration in the early part of the machine and reduce the number of beams.

The modulators in a recirculator will be different from those chosen in any of the linac approaches. In the linac examples, a voltage pulse is a applied to the core just once per "shot" so the repetition rate is the rate at which the fusion targets are shot, a few Hz. In the recirculator example the cores are fired once each lap, so repetition rates up to of order 100 kHz are required. Further, as the beam accelerates, the pulse repetition rate increases, and because of the velocity increase and bunch compression the pulse duration decreases. The modulators on a linac are envisioned as pulse forming networks of capacitors and inductors, which form a pulse of a fixed duration and fixed waveform, after being initiated by a high-power switch such as a thyratron. The recirculator designs use capacitors for energy storage, which are discharged using arrays of solid state switches (MOSFETS), to both initiate and terminate the pulse. Arrays are required because many switches are required in series to hold the required voltage, and in parallel to carry the required current. Although, arrays of solid-state switches are individually more expensive than the pulse forming network approach, the smaller number of modulators required in a recirculator permits their use, despite their higher unit cost.

For a fusion power plant to be practical, the driver must be highly efficient in converting wall plug power into beam power. Efficiencies in the range of 20–30% are calculated to be possible using induction acceleration. One of the main sources of energy loss in induction linacs is dissipative losses in the induction cores. "Eddy current" losses arise when inductive electric fields within the cores create currents, producing resistive losses. Again using Faraday's law, the inductive field E is proportional to geometric factors times $\partial B/\partial t \cong \Delta B/\Delta t$. The current density J is given by $J = \sigma_c E$, where σ_c is the conductivity, so that the power lost per unit volume is proportional to $J \cdot E \sim \sigma_c E^2 \sim \Delta B^2/\Delta t^2$. Over the course of a pulse of duration Δt the energy dissipated per unit volume is thus proportional to $\sigma_c \Delta B^2/\Delta t$. Although this model omits anomalous effects due to domain wall motion, the scaling of loss with $\Delta B^2/\Delta t$ is a reasonable match to data at large $\Delta B/\Delta t$ [8].

As the pulse duration gets very long, the eddy current losses go toward zero. Hysteresis losses contribute a second form of energy loss. This is the energy required to reorient the domains of magnetic flux along the imposed field direction. As the rate of change of the flux goes to zero this loss approaches a value proportional to the total change in flux ΔB. Empirically, the losses per unit volume $\mathscr{L}$ can be expressed approximately as in Ref. [8]:

$$\mathscr{L} \cong 750\left(\frac{\Delta B}{2.5\mathrm{T}}\right)^2\left(\frac{1\ \mu\mathrm{s}}{\Delta t}\right) + 100\left(\frac{\Delta B}{2.5\mathrm{T}}\right)\mathrm{J/m^3}. \tag{2}$$

Consider an accelerator that has a constant acceleration gradient $\mathrm{d}V/\mathrm{d}s = (V_f - V_i)/N_{gap}L$. Here subscripts i and f indicate initial and final values, respectively, and N_{gap} is the number of accelerating cores encountered by the beam (which for a recirculator is equal to the number of turns times the

number of half-lattice periods in the ring). As an illustration we consider a pulse duration that decreases linearly with distance (or voltage), so that

$$\Delta t = \Delta t_{\rm i} + (\Delta t_{\rm f} - \Delta t_{\rm i})(V - V_{\rm i})/(V_{\rm f} - V_{\rm i}). \quad (3)$$

In that case, the total loss in the inductive cores $\mathscr{L}_{\rm tot}$, under these assumptions is given by

$$\mathscr{L}_{\rm tot} = \left[4.7\ {\rm MJ} \left(\frac{{\rm d}V/{\rm d}s}{1\ {\rm MV/m}}\right)\left(\frac{0.5\ {\rm m}}{R_{\rm out} - R_{\rm in}}\right)\left(\frac{0.8}{\eta_{\rm core}}\right) + 0.63\ {\rm MJ} \right] \times \left(\frac{R_{\rm out} + R_{\rm in}}{1\ {\rm m}}\right)\left(\frac{V_{\rm f} - V_{\rm i}}{10\ {\rm GV}}\right)\left(\frac{\Delta t_{\rm i} + \Delta t_{\rm f}}{1\ \mu s}\right).$$

Here, the core inner and outer radii are given by $R_{\rm in}$ and $R_{\rm out}$, respectively, and $\eta_{\rm core}$ is the ratio of the core length to the distance between accelerating gaps. Note that core losses can be reduced by going to small accelerating gradients and by increasing core volume so that the cores operate away from saturation. Both effects will reduce the first term in $\mathscr{L}_{\rm tot}$, and can be carried out until hysteresis dominates the core loss. The recirculator operates at a much lower accelerating gradient and therefore will have more efficient acceleration. High-charge state machines have much lower $V_{\rm f}$ and therefore will also have more efficient acceleration.

In recirculators, a second major source of energy loss is present. As the energy of the beam increases during the acceleration of a beam pulse, so too must the dipole field which bends the beam. The scale over which the acceleration occurs is a few milliseconds, which is faster than the permissible ramping time of present-day superconducting magnets. Conventional magnets must be used, with losses generally proportional to the magnetic field energy (proportional the square of the field B.) In the magnets under consideration for recirculators, losses arise from four major sources [9]. These are: (1) resistive losses in the conducting wire coils, (proportional to $I^2RP \sim B^2P$, where I is the current, R is the wire resistance, and P is the residence time of the beam within the ring); (2) eddy currents within the conductors ($\sim B^2x^3/P$ where x is the width of the wire); (3) eddy current losses in the laminated iron yokes needed to confine and direct the magnet flux (also proportional to B^2/P); and (4) hysteresis loss in the iron. In driver recirculator designs ~ 40 MJ of magnetic energy is stored in the magnetic field. Efficient recovery of this energy for subsequent pulses is required to achieve overall high efficiency of the accelerator. Dipole designs (including the effects of cooling channels) in which $\sim 90\%$ of the magnetic energy is reused each pulse appear achievable.

3. Scaling of the focusing systems

In the absence of acceleration, the envelope equations for the three focusing systems may be written:

$$\frac{{\rm d}^2 a}{{\rm d}s^2} = \frac{\varepsilon^2}{a^3} + \begin{cases} \dfrac{2K}{a+b} \pm \dfrac{V_{\rm q}}{V}\dfrac{a}{r_p^2} & \text{Electric quads,} \\ \dfrac{2K}{a+b} \pm \left(\dfrac{qB_q^2}{2{\rm mV}}\right)^{1/2}\dfrac{a}{r_p} & \text{Magnetic quads,} \\ \dfrac{K}{a} + \dfrac{\omega^2 a}{v_z^2} - \dfrac{\omega\omega_c a}{2v_z^2} & \text{Solenoids.} \end{cases} \quad (4)$$

Here a is the envelope radius in the x-direction, $K = \lambda/4\pi\varepsilon_0$ is the perveance, qV is the particle energy, q and m are the charge and mass of the particle, ω is the rotation frequency of the beam envelope, $\omega_{\rm c}$ is the cyclotron frequency, ε is the unnormalized beam emittance, v_z is the axial beam velocity, and $r_{\rm p}$ is the aperture (beam-pipe) radius. For the quadrupole case, the equation for the envelope radius in the y-direction b, is found by interchanging a with b in Eq. (4). For the solenoid case, the beam is axisymmetric, so that $a = b$. Also in the solenoid case, the focusing results from the difference between the outward centrifugal force due to beam rotation and the inwardly directed $v_\theta B_z$ force, where v_θ is the azimuthal beam rotation velocity and B_z is the solenoidal magnetic field. In addition, space charge and emittance tend to defocus the beam.

In the quadrupole case the beam alternately receives "kicks" which focus then defocus, but since the focusing occurs when the beam is at larger radius where the kicks are stronger, there is an average net focusing. We may average over a lattice period to obtain a smooth approximation to the focusing [10]. In the solenoid case, we may maximize the focusing by choosing $\omega = \omega_{\rm c}/2$. Then, all three focusing systems may be represented approximately by an envelope equation for the average

beam radius a,

$$\frac{\mathrm{d}^2 a}{\mathrm{d}s^2} = \frac{\varepsilon^2}{a^3} + \frac{K}{a} - k^2 a. \tag{5}$$

Here,

$$k^2 = \begin{cases} \dfrac{1}{4r_p^2}\left(\dfrac{\eta_q L}{r_p}\right)^2 \dfrac{V_q^2}{V^2} & \text{Electric quad,} \\ \dfrac{1}{8}\left(\dfrac{\eta_q L}{r_p}\right)^2 \left(\dfrac{qB_q^2}{\mathrm{mV}}\right) & \text{Magnetic quad,} \\ \dfrac{\eta_s}{8}\left(\dfrac{qB_s^2}{\mathrm{mV}}\right) & \text{Solenoid.} \end{cases} \tag{6}$$

Here η_q is the quadrupole occupancy, and η_s is the solenoid occupancy. Note that for electrostatic quads k^2 is proportional to $1/V^2$ whereas for magnetic quads k^2 varies as $1/V$ suggesting that at low voltages electrostatic quads will be more effective than magnetic quads. Note also that for quadrupole focusing the focusing constant increases as the lattice period increases, whereas for solenoids the constant is independent of lattice period.

The particle undergoes quasi-harmonic betatron motion with wave number k. The phase advance (in the absence of spacecharge) σ_0 is approximately given by $\sigma_0 = 2\,kL$ designated per lattice period $2L$. Note that for aligned solenoids the period $2L$ contains a single magnet, but two magnets for alternating solenoids, whereas there are two quadrupoles in period $2L$.

For all three systems, the phase advance cannot be made arbitrarily large. Envelope/lattice instabilities set in for $\sigma_0 \gtrsim \pi/2$ [11].

By eliminating the lattice period $2L$ in favor of σ_0, and equating the space charge term K/a to the focusing term $k^2 a$ in Eq. (5) (ignoring the normally small contribution from the emittance term), we may calculate the maximum transportable line charge density per beam λ_b. This is one form of the so-called "Maschke limit".

Here e and m_H are the charge and mass of the proton, respectively. We note that the line charge density limit per beam λ_b increases with voltage V only for the magnetic quadrupoles, which leads to the choice of magnetic quadrupoles for the high energy section in all four example concepts described here. Note also that, although the line charge density limit for the solenoids has a smaller coefficient at the nominal values of the field and pipe radius indicated, λ_b increases with the square of $B_s r_p$, whereas for the quads it rises linearly with $B_q r_p$.

Also note that λ_b is independent of r_p for electrostatic quads, proportional to r_p for magnetic quads, and r_p^2 for solenoids. We define a second relevant quantity λ_tot equal to the total line charge that can be transported through an induction core of fixed inner radius R. We follow the argument of Ref. [12], adding solenoidal focusing to the discussion.

The number of beams N_b threading each induction core is proportional to $(R/r_q)^2$ where r_q is the outer radius of the quadrupole or solenoid (for large N_b). Assuming that r_q/r_p is constant as one changes the number of beams, then the total transportable line charge $\lambda_\mathrm{tot} \sim V_q N_b$ for electric quads, $B_\mathrm{q} N_\mathrm{b}^{1/2}$ for magnetic quads, B_s^2 for solenoids. Further, $V_q \sim r_p^{1/2\text{ to }1}$ to avoid breakdown, and for small magnetic field values B_q and B_s are proportional to I_m/r_p where I_m is the total current in the magnet. But $I_m \sim J_\mathrm{crit} r_p^2$ where J_crit is the critical current density for superconducting magnets, and is assumed here to be only weakly dependent on field strength. Thus B_q and B_s are proportional to r_p for fixed ratio r_q/r_p which suggests that $\lambda_\mathrm{tot} \sim N_b^0$ (for magnetic quads) and $\lambda_\mathrm{tot} \sim N_b^{-1}$ (solenoids). For large r_p and magnetic fields, for technological and economic reasons the magnets are designed at nearly constant maximum values, so that $\lambda_\mathrm{tot} \sim N_b^{1/2}$ (for magnetic quads) and

$$\lambda_b = \begin{cases} 0.9\,\dfrac{\mu\mathrm{C}}{\mathrm{m}}\left(\dfrac{\sigma_0}{1.4}\right)\left(\dfrac{a/r_p}{0.7}\right)^2\left(\dfrac{\eta}{0.7}\right)\left(\dfrac{V_q}{80\mathrm{kV}}\right) & \text{Electric quads,} \\ 1.0\,\dfrac{\mu\mathrm{C}}{\mathrm{m}}\left(\dfrac{\sigma_0}{1.4}\right)\left(\dfrac{a/r_p}{0.7}\right)^2\left(\dfrac{\eta}{0.7}\right)\left(\dfrac{B_q}{2T}\right)\left(\dfrac{qm_\mathrm{H}/em}{1/200}\right)^{1/2}\left(\dfrac{V}{2\ \mathrm{MeV}}\right)^{1/2}\left(\dfrac{r_p}{6\ \mathrm{cm}}\right) & \text{Magnetic Quads,} \\ 0.03\dfrac{\mu\mathrm{C}}{\mathrm{m}}\left(\dfrac{a/r_p}{0.7}\right)^2\left(\dfrac{\eta}{0.7}\right)\left(\dfrac{B_s}{2T}\right)^2\left(\dfrac{q/em}{1/200}\right)\left(\dfrac{r_p}{6\,\mathrm{cm}}\right)^2 & \text{Solenoids.} \end{cases} \tag{7}$$

$\lambda_{\rm tot} \sim N_b^0$ (solenoids). Summarizing these scalings, we find

$$\lambda_{\rm tot} \sim \begin{cases} N_{\rm b}^{1/2 \text{ to } 3/4} & \text{Electric quads,} \\ N_{\rm b}^{0 \text{ to } 1/2} & \text{Magnetic quads,} \\ N_{\rm b}^{-1 \text{ to } 0} & \text{Solenoids.} \end{cases} \quad (8)$$

From Eq. (7), it is apparent that for electrostatic quads a larger number of beams is optimal, for magnetic quads larger numbers of beamlines are somewhat favored, but for solenoids a smaller number of beamlines will be optimal. Indeed, (a/r_p) multiplies the above expression, and since finite alignment precision suggests that a/r_p tends to zero as a tends to zero (or $N_{\rm b}$ tends infinity), even for electric quads an upper limit on the number of beams for maximum transportable current is reached. It is thus apparent how the scaling of transportable current leads to a large number of beams in accelerators with electric quadrupole "front ends", and a small number of beams in an accelerator with solenoids in the low energy section.

4. Accelerator scaling with charge-to-mass ratio

In order to obtain a qualitative understanding of how accelerator costs scale with charge-to-mass ratio q/m we may consider a simplified example using quadrupole transport to illustrate the scaling. In comparing drivers which use different charge-to-mass ratios, target requirements constrain the driver to maintain the same pulse energy $QV_{\rm f}$, the same pulse duration at the target $\Delta t_{\rm t}$, and the same ion range R. Here Q is the total charge in the bunch, and $qV_{\rm f}$ is the final ion energy. A crude low-order approximation (but sufficient for our purposes) of the mass and energy dependence of the range R is that R depends only on β where βc is the ion velocity. (This neglects a slow decrease in range as the atomic mass increases, at fixed β).

Under these assumptions $qV_{\rm f}/m \cong$ constant. This directly implies that $V_{\rm f} \sim m/q$ and $Q \sim q/m$. For a linac the accelerator length $L_{\rm acc}$ decreases for large q/m since $L_{\rm acc} \sim V_{\rm f}/({\rm d}V/{\rm d}s) \sim m/q$. Here ${\rm d}V/{\rm d}s$ is the maximum accelerating gradient, which is typically set at 1–2 MVm. For larger q/m the space charge increases. For a concrete comparison, we make the additional assumption that the voltage, pulse duration, and geometry of the injector (such as r_p) are fixed, but that as q/m is altered the number of beams changes to account for the changes in required space charge. Under those assumptions

$N_{\rm bi} \sim Q/l_{\rm bi}\lambda_{\rm bi} \sim (q/m)^{1/2}$ Electric quads,

$N_{\rm bf} \sim Q/l_{\rm bf}\lambda_{\rm bf} \sim (q/m)$ Magnetic quads,

Above $Q \sim q/m$, $l_{\rm bi} \sim (q/m)^{1/2}$, $\lambda_{\rm bi} \sim 1$ (for electric quads), and $\lambda_{\rm bf} \sim 1$ (for magnetic quads), and where subscripts i and f represent initial and final, respectively.

We again assume for this example that the pulse duration decreases linearly with distance (Eq. (3)). The required total volt-second capability of the accelerator is given by $\int \Delta t({\rm d}V/{\rm d}s)\,{\rm d}s = \int \Delta t\,{\rm d}V \sim m/q$. Hence the inner radius of core $\sim N_{\rm b}^{1/2} \sim (q/m)^{1/2 \text{ to } 1/4}$, and the total core volume and costs $\sim (m/q)^{1/2 \text{ to } 3/4}$. This result suggests that there will be a cost savings associated with larger q/m. As will be discussed in the next section, the challenges for this approach arise from more stringent requirements at the final focus and at the injector.

5. Phase-space constraints set by final focus

In order to achieve high gain the beam must be focused onto a small spot of radius $r_{\rm s}$ at the target. We summarize below constraints on the beam assuming unneutralized ballistic transport to the target, (see e.g. Ref. [13]).

When focusing the beam through a final convergent angle θ, space charge limits the final beam radius. This limit can be expressed as a minimum number of beams required to focus each beam within a spot $r_{\rm s}$:

$$N_{\rm b} > Q \ln(\theta d/r_{\rm s})/(2\pi\varepsilon_0\theta^2 V\beta c\,\Delta t_{\rm t}).$$

For the recirculator design of Ref. [2] with a total charge Q in all beams of 400 μC, convergence angle $\theta = 0.03$ and $\beta = 0.3$ (corresponding to 10 GeV), $N_{\rm b}$ could be as small as 4. For the multi-beam linac at lower energy (4 GeV) and higher total charge (1650 μC), and smaller convergence angle $\theta = 0.015$, ~ 220 beams would be required. Using the scaling of Section 4, $N_{\rm b} \sim (q/m)^2$, so that

neutralization is almost certainly required for charge states above 1.

The thermal contribution to spot size places a limit on the normalized emittance ε_N: $\varepsilon_N < \beta\theta r_s = 8$ mm mrad$(\beta/0.2)$ $(\theta/0.015)$ $(r_s/2.5$ mm$)$. Chromatic aberration limits for transport through quadrupole lenses place a limit on the momentum spread: $\Delta p/p < r_s/6\theta d = 3\times 10^{-3}$ $(r_s/2.5$ mm$)$ $(0.015/\theta)$ $(5$ m$/d)$, where d is the distance from target to final focusing magnet. Geometric aberrations limit the convergent angle for uncorrected optics, $\theta < 0.015$ rad (cf. Ref. [14]). Using octupoles, Ref. [15], it was found that this limit could be relaxed, and designs as large as $\theta = 0.030$ have been considered.

The target power requirements place limits on the 3D space coordinates of the beam (pulse length and beam radius r_s) while final focus optics place constraints on the 3D momentum coordinates ($\Delta p/p$ and ε_{nx}/r_s and ε_{ny}/r_s), necessary to reach the spot radius r_s. Additionally, because of Liouvilles theorem, the final 6D phase volume occupied by the beam will be at least as large as the initial volume. This constraint can be expressed by a "dilution factor" D (cf. Ref. [16]), which is a ratio of the initial to final 6D volumes and is a measure of how much room for emittance dilution exists in any particular driver concept.

$$D = \frac{\varepsilon_{Nf}^2 \Delta p_f l_f}{\varepsilon_{Ni}^2 \Delta p_i l_i}. \tag{9}$$

Here l_i and l_f are the initial and final bunch lengths of the beam. If we assume the focusing limits on emittance and momentum spread discussed above, for the recirculator in [2] (in which $\varepsilon_{Nf} < 8$ mm mrad, $\varepsilon_{Ni} = 0.5$ mm mrad, $p_i/p_f = 1.7\times 10^{-2}$, $l_f = 1$ m, $l_i = 340$ m, $\Delta p/p_f < 1.4\times 10^{-3}$, and $\Delta p/p_i > \sim 10^{-3}$ from assumed voltage errors in the injector), we find that there is phase-space dilution allowance $D \cong 62$, which allows for only a factor of 4 growth in phase area in each of the three directions. This relatively small leeway is largely a result of the large initial pulse duration chosen in the recirculator, to reduce the number of beams. As one increases the number of beams as in the linac designs the constraint relaxes. In the multi-charge state example given in Section 4, the injector voltage and pulse duration were held constant, for the concrete example discussed in that section. Under this assumption, the initial velocity increases, and so the initial bunch length does as well, similar to the recirculator, which implies the high charge state linac is also fairly constrained relative to the single charge multibeam linac. (Note that $D > 1$ is a minimum requirement. If coupling between the transverse and longitudinal directions is not sufficiently strong, the areas of individual phase space projections in each direction (i.e. ε_{Nx}, ε_{Ny}, or Δpl) will individually be non-decreasing, which in some cases can result in a stronger constraint on allowable emittance dilution).

6. Comparison of the four example induction accelerators

6.1. Multiple-beam quadrupole-focused linacs

The multi-beam linac is currently the mainline approach to inertial fusion drivers in the US. Of the four examples, it is the closest match to existing technology. The multiple beam approach is chosen to meet the target requirements based on space charge and phase-space density constraints. Recently, Meier et al. [1] have been developing a systems code which will put each of the various accelerator configurations onto a common cost and efficiency basis. They have recently applied the code to a design that is specifically tailored to a recent LLNL target design [5]. The design consists of an electrostatic quadrupole front end with 192 beams (injected with a pulse energy of 2 MeV and pulse duration of 30 μs.) The beams undergo a four-to-one merge at the 100 MeV point into 48 beams transported by magnetic quads. Since the target requires a prepulse at lower energy (3 GeV), once that energy is reached, 16 of the beamlines are transported outside the main induction cores while the remaining 32 beams continue acceleration to 4 GeV. The main pulse exits the accelerator at 108 ns and undergoes drift compression, reaching 8 ns at the target. (The prepulse is similarly compressed from 143 to 30 ns).

There are a number of key physics and technology issues associated with the multibeam linac

concept. (1) Control and alignment of multiple-beam arrays needs validation. Since there have been few experiments with such large arrays of ion beams, there have been few attempts to quantify the requirements on control system complexity and alignment. (2) Transport of beams with large head-to-tail velocity tilt needs assessment. This is a question which affects all four of the concepts and ultimately becomes a question of what velocity tilt can be transported without inducing mismatch oscillations on the beam. (3) Inter-beam interactions in gaps is another area needing further research. In a high gradient machine the acceleration gaps are either longer or are graded, making this issue more important for this concept. Methods for shielding the beams within the gaps need to be assessed. (4) Emittance dilution from merging is ultimately an issue of system optimization (some designs have, in fact, no merging), since the emittance dilution associated with a beam merge must be accounted for in an optimized design. Simulations and recent experiments will help resolve this issue. (5) The final uncertainty (which applies to all concepts) is cost.

6.2. Recirculators

The recirculator as envisioned in Ref. [2] consisted of several rings, each increasing the energy by a factor of about 10 and decreasing the pulse duration by a factor of about three. The prime motivation for the study was to see if it was possible to substantially reduce the cost of the accelerator relative to a linac design. Further, the authors tried to design a machine with a small number of beams, favoring the simplicity of four beams relative to the complexity of the large number of beams in the linac approach, and eliminating the need to merge beams with the associated emittance growth. Designing a machine with fewer beams, however, meant the design relied on large initial pulse durations in order to satisfy the constraint of Eq. (6). Since the recirculator can operate at a reduced acceleration gradient (because the accelerator components are reused over the course of ~ 100 turns), long pulse durations can be entertained more easily in a recirculator than in a linac, without requiring very large induction cores (cf. Eq. (1)).

However, because of the smaller accelerating gradient, the beam covers a much larger path length. Beam loss from residual gas and charge-changing collisions of beam particles with each other are more problematic in a recirculator, and the poorly understood effects of lost beam and ionized residual gas hitting the wall, producing addititonal outgassing (a beam intensity dependent effect) needs experimental verification to establish that the vacuum behaves as predicted. As indicated above, the efficiency of ramped dipoles is crucial to the recirculator design, since the recycled dipole energy is larger than the beam energy itself. Insertion/extraction of multiple beams into and out of the ring also requires validation. In Ref. [2] the beam lines were arrayed in a square pattern within the bend sections (to minimize core volume) but were arrayed vertically in the insertion/extraction section to facilitate use of the rectangular quads used for getting the beam into and out of the ring. This arrangement allowed path equalizing exchange of inner beams with outer beams in the bends. Use of superconducting quadrupoles provides an efficient focusing system and constant magnetic field. As the beam accelerates, the tune changes rapidly, effectively passing through resonances. As a result, the recirculator operates in a space charge dominated regime, far exceeding the Laslett tune shift limit of conventional circular accelerators. Validation of this operation point experimentally is a key goal of the bending and recirculation experiments taking place at LLNL [17]. Finally, the long pulse durations which enabled a small number of beams to be accelerated at the beginning of the accelerator, imply larger momentum spread at the end of the accelerator, so there is less leeway for phase space dilution. Injectors with smaller voltage errors or achromatic final focusing systems would be beneficial to recirculators with long initial pulse duration. Also, recirculators with more beams and shorter pulses (hence closer in concept to "circular" linacs) are being evaluated.

6.3. Solenoidal focus linac

As discussed earlier, a linac with a solenoidally focused low-energy section has been considered

because of a potential cost reduction associated with fewer beams, a simpler control system and less complicated inter-beam interactions. Further, the risks associated with merging beams are not present. In Ref. [3], advantage was taken of the quadratic scaling of line charge with magnetic field, to suggest a four beam system, each with a 10 T solenoidal field, and beam radius of 10 cm. The solenoids would extend from 4 MeV (and 10 μs) to 30 MeV (with a pulse duration of 3.7 μs), after which the magnetic quads would transport the beam to 4 GeV (and 132 ns) with a total pulse energy in all beams of 4 MJ.

There are a number of key issues associated with this concept. The large source required for the injector. No experience with such sources has as of yet been obtained. A second major concern is aberrations from the fringe fields of laterally adjacent solenoids. Multiple beam arrays are not as naturally compatible as they are with quadrupoles. With solenoids, the flux through the end of one solenoid interacts in a non-axisymmetric manner with the flux from an adjacent one, producing large non-linear field aberrations, unless the flux from the solenoids is contained or they are separated a sufficient distance. An alternate concept is to provide induction cores around each solenoid, paying the cost penalty for the additional core material. A third issue is the control of backflowing electrons flowing down magnetic field lines and achieving high energy going through multiple gaps. Alternating the field direction longitudinally (as is often done in electron beams) is one potential solution. In a quad system electrons are blocked axially because the fields are primarily transverse. A fourth issue is the small number of beams at the target. In the four-beam scenario charge neutralization would be required to focus the beams.

6.4. High charge state, multiple induction coreline linac

The final induction accelerator example discussed here is the high charge state, multiple coreline linac. An example of one of the designs in Ref. [4] consists of 14 corelines, each with 7 beams of Xenon^{+8} (atomic mass 131). The total ion energy is 2.09 GeV, corresponding to a voltage of only 261 MeV, achieved in less than 300 m. The source would be a cryogenic noble gas target, a few mm in radius. The spherical ion source pellet is produced by injecting a 10 μm radius solid sphere of cryogenic Xe and illuminating it by a laser prepulse that heats the solid into an expanding gaseous state. When the gas reaches a radius of a few mm, a 100 fs, 100 TW laser ionizes the gas to a nearly pure ionization state of $+8$. This method has the potential advantage of producing a beam of low emittance and pure charge state. The advantages of the machine are the reduction in development cost by building a full-scale prototype beamline. This design also takes advantage of recent ultra-short-pulse laser advancements as an enabling technology for the injector of such a machine.

The key issues for this machine are the emittance and charge state purity of the source and phase-space density constraints, discussed in Section 5. The other major issue which comes about because of the high charge state, is the plasma neutralization of beam space charge during final drift compression and final focus. This neutralization is necessarily required, and both operations are more uncertain than in the singly charged multi-beam linac approach to HIF, and in fact require significant research to develop the operations themselves.

7. Conclusions

We are narrowing down the options for a heavy-ion fusion driver. A systems code which places all of these options on a common cost basis and also uses the same algorithms for calculating energy loss is being developed (cf. Ref. [1]). Scaled experiments such as being done for beam combining Ref. [18] and recirculation, Refs. [17,19] are being carried out to reduce uncertainties in technical risk. Technology development and assessment (such as the Metglas studies of Ref. [8]) are also being carried out to understand the performance and energy loss properties of key elements of induction machines. The four concepts discussed in this paper represent classes of machines. Hybrids between the classes will be also be assessed using the systems codes. The ultimate goal of all of these studies will be an

affordable development path toward a cost-effective driver for heavy ion fusion, and therefore clean and inexpensive generation of electric power.

References

[1] W.R. Meier, R.O. Bangerter, A. Faltens, Nucl. Instr. and Meth. A 415 (1998) 249.

[2] J.J. Barnard, A.L. Brooks, J.P. Clay, F.J. Deadrick, L.V. Griffith, A.R. Harvey, D.L. Judd, H.C. Kirbie, V.K. Neil, M.A. Newton, A.C. Paul, L.L. Reginato, G.E. Russell, W.M. Sharp, H.D. Shay, J.H. Wilson, S.S. Yu, UCRL-LR-108095, Recirculating Induction Accelerators as Drivers for Heavy Ion Fusion, Lawrence Livermore National Laboratory (1991); also J.J. Barnard, F. Deadrick, A. Friedman, D.P. Grote, L.V. Griffith, H.C. Kirbie, V.K. Neil, M.A. Newton, A.C. Paul, W.M. Sharp, H.D. Shay, R.O. Bangerter, A. Faltens, C.G. Fong, D.L. Judd, E.P. Lee, L.L. Reginato, S.S. Yu, T.F Godlove, Physics of Fluids B: Plasma Physics 5 (1993) 2698.

[3] E.P. Lee, R.J. Briggs, The solenoidal transport option: IFE drivers, near term research facilities, and beam dynamics, LBNL 40774, UC-419, September, 1997. Nucl. Instr. and Meth. A 415 (1998) 274.

[4] B.G. Logan, M.D. Perry, G.J. Caporaso, Concept for high-charge-state ion induction accelerators, International Atomic Energy Agency Technical Committee Meeting on Drivers and Ignition Facilities for Inertial Fusion, Osaka, Japan, 10–14 March, 1997.

[5] M. Tabak, D. Callahan-Miller, Nucl. Instr. and Meth. A (1998) 75.

[6] LBL HIF Staff, Linear induction accelerator conceptual design, HIFAN 58, Sept. 1978.

[7] S. Humphries Jr., Principles of Charged Particle Acceleration, chs. 5 and 10, Wiley, New York, 1986.

[8] A.W. Molvik, A. Faltens, L. Reginato, M. Blaszkiewicz, C. Smith, R. Wood, Nucl. Instr. and Meth. A 415 (1998) 315.

[9] T.F. Godlove, Particle Accelerators 37–38 (1992) 439.

[10] M. Reiser, Particle Accelerators 8 (1978) 167.

[11] I. Hofmann, L.J. Laslett, L. Smith, I. Haber, Particle Accelerators 13 (1983) 145.

[12] R.O. Bangerter, Il Nuovo Cimento 106, 1445.

[13] D.A. Callahan, Fusion Eng. Des. 32 (1996) 441.

[14] D. Neuffer, Geometric aberrations in final focussing for heavy ion fusion, Proc. HIF Workshop Held at Argonne National Laboratory, 19–26, Sept. 1978, ANL-79-41, (1979) p. 333.

[15] D.D.- M Ho, I. Haber, K.R. Crandell, Particle Accelerators 36 (1991) 141.

[16] D. Judd, Phase space constraints on some heavy-ion inertial-fusion igniters and example designs of 1 MJ RF LINAC systems, Proc. Heavy Ion Fusion Workshop Held at Argonne National Laboratory, 19–26 September 1978, ANL-79-41, p. 237.

[17] T.C. Sangster, J.J. Barnard, V. Cianciolo, G.D. Craig, A. Friedman, D.P. Grote, E. Halaxa, R.L. Hanks, G. Kamin, H.C. Kirbie, B.G. Logan, S.M. Lund, G. Mant, W. Manning, A.W. Molvik, M.B. Nelson, W.M. Sharp, T.J. Fessenden, D.L. Judd, L. Reginato, D. Berners, H.A. Hopkins, A. Debeling, J. Meredith, Nucl. Instr. and Meth. A 415 (1998) 310.

[18] P.A. Seidl, C.M. Celata, A. Faltens, W.H. Fawley, W. Ghiorso, S. Maclaren, Nucl. Instr. and Meth. A 415 (1998) 243.

[19] J.G. Wang, S. Bernal, P. Chin, R. Kishek, Y. Li, M. Reiser, M. Venturini, Y. Zou, T.F. Godlove, I. Haber, R.C. York, Nucl. Instr. and Meth. A 415 (1998) 422.